Draft version January 13, 2016
Preprint typeset using LaTeX style emulateapj v. 5/2/11

arXiv:1601.02614v1 [astro-ph.IM] 11 Jan 2016

APODIZED PUPIL LYOT CORONAGRAPHS FOR ARBITRARY APERTURES. V. HYBRID SHAPED PUPIL DESIGNS FOR IMAGING EARTH-LIKE PLANETS WITH FUTURE SPACE OBSERVATORIES

Mamadou N'Diaye[1], Rémi Soummer[1], Laurent Pueyo[1], Alexis Carlotti[2], Christopher C. Stark[1], Marshall D. Perrin[1]

Draft version January 13, 2016

ABSTRACT

We introduce a new class of solutions for Apodized Pupil Lyot Coronagraphs (APLC) with segmented aperture telescopes to remove broadband diffracted light from a star with a contrast level of 10^{10}. These new coronagraphs provide a key advance to enabling direct imaging and spectroscopy of Earth twins with future large space missions. Building on shaped pupil (SP) apodization optimizations, our approach enables two-dimensional optimizations of the system to address any aperture features such as central obstruction, support structures or segment gaps. We illustrate the technique with a design that could reach 10^{10} contrast level at 34 mas for a 12 m segmented telescope over a 10% bandpass centered at a wavelength λ_0 =500 nm. These designs can be optimized specifically for the presence of a resolved star, and in our example, for stellar angular size up to 1.1 mas. This would allow probing the vicinity of Sun-like stars located beyond 4.4 pc, therefore fully retiring this concern. If the fraction of stars with Earth-like planets is $\eta_\oplus = 0.1$, with 18% throughput, assuming a perfect, stable wavefront and considering photon noise only, 12.5 exo-Earth candidates could be detected around nearby stars with this design and a 12 m space telescope during a five-year mission with two years dedicated to exo-Earth detection (one total year of exposure time and another year of overheads). Our new hybrid APLC/SP solutions represent the first numerical solution of a coronagraph based on existing mask technologies and compatible with segmented apertures, and that can provide contrast compatible with detecting and studying Earth-like planets around nearby stars. They represent an important step forward towards enabling these science goals with future large space missions.

Subject headings: Instrumentation: high angular resolution – Techniques: high angular resolution – Telescopes – Methods: numerical

1. INTRODUCTION

Discovering and studying nearby Earth twins with direct imaging and spectroscopy requires a telescope large enough to provide sufficient angular resolution and sensitivity to planets around a significant sample of stars (e.g. Stark et al. 2014). These exoplanet goals align well with other general Astrophysics needs, and large space missions are being proposed and studied by NASA and by the community (e.g. Large UV/Optical/IR (LUVOIR), Advanced Technologies Large Aperture Space Telescope (ATLAST), and High Definisiton Space Telescope (HDST)[3] Postman et al. 2012; Kouveliotou et al. 2014; Feinberg et al. 2014).

Because of launch systems limitations, segmented apertures are unavoidable for space telescopes larger than 8 m typically. For starlight attenuation two types of architectures can be considered: external occulters and internal coronagraphs. External occulters, such as EXO-S[4] are promising solutions for exoplanet imaging and spectroscopy, with advantageous high throughput and broadband capabilities. However, for a large aperture their operations become very inefficient as their size, mass and repointing times, scale with the aperture diameter (Savransky et al. 2010; Redding et al. 2014). In this context internal coronagraphs represent a theoretically more attractive solution for very large telescopes, but aperture discontinuities (primary mirror segmentation, central obstruction, spiders) make high-contrast imaging extraordinarily challenging with two particular major issues: starlight suppression, and high-contrast stability during observations. Given the complexity of the problem, a systemic approach is necessary to combine wavefront sensing and control for segment co-phasing and low-order aberration measurements (e.g. Guyon et al. 2009; Mas et al. 2012; N'Diaye et al. 2013a; Singh et al. 2014), coronagraphy for starlight diffraction suppression (e.g. see review in Guyon et al. 2006), and wavefront control for the generation and stabilization of the high-contrast dark region in the image (e.g. using two deformable mirror based methods, Shaklan & Green 2006; Pueyo & Kasdin 2007; Pueyo et al. 2009; Thomas et al. 2015). Over the past couple of years, different research studies and laboratory testbeds were initiated to study such integrated solutions for future large space or ground-based observatories (N'Diaye et al. 2013b, 2014, 2015b; Galicher et al. 2014; Hicks et al. 2014; Martinez et al. 2014; Miller et al. 2015).

For many years, coronagraphs studies have focused on developing technologies for monolithic, off-axis telescopes. Recent progress in design and component fabrication (e.g. Balasubramanian et al. 2013; Delacroix et al. 2013; Otten et al. 2014; Newman et al. 2015) have allowed the community to jump over the first major hurdles, and contrasts beyond 10^9 levels have been achieved in laboratory (see review in Mawet et al. 2012). These coronagraph designs are particularly compelling for small off-axis space telescopes that have been proposed over the past few years to observe a few hundreds of targets, directly image and characterize extrasolar planets and circumstellar disks (e.g. EPIC, ACCESS, PECO, SPICES, EXO-C[5] Clampin et al. 2006; Trauger et al. 2010; Guyon et al.

[1] Space Telescope Science Institute, 3700 San Martin Drive, 21218 Baltimore MD, USA
[2] CNRS, IPAG, F-38000 Grenoble, France

[3] http://www.hdstvision.org/report/

[4] http://exep.jpl.nasa.gov/stdt/Exo-S_Starshade_Probe_Class_Final_Report_150312_URS250118.pdf

[5] http://exep.jpl.nasa.gov/stdt/Exo-C_Final_Report_for_Unlimited_Release_150323.pdf

2010b; Boccaletti et al. 2012; Stapelfeldt et al. 2014). However most of these concepts are unable to perform with a large on-axis segmented telescope.

With the development of the WFIRST-AFTA mission and its coronagraphic instrument (Spergel et al. 2015; Zhao 2014), the focus has shifted to include investigations of coronagraph designs that can handle on-axis telescopes with pupil features, such as large central obstruction and support structures. Several classic coronagraphic concepts have been revisited over the past two years (Baudoz et al. 2000; Rouan et al. 2000; Kuchner & Traub 2002; Kasdin et al. 2003; Mennesson et al. 2003; Mawet et al. 2005; Lyon et al. 2006; Guyon et al. 2010a) and novel designs have emerged to push their performance further with arbitrary apertures (Balasubramanian 2008; Carlotti et al. 2011; Mawet et al. 2013; Guyon et al. 2014; Carlotti 2013; Carlotti et al. 2014; Lyon et al. 2015). In addition to the coronagraph itself, pupil remapping techniques (Pueyo & Norman 2013; Mazoyer et al. submitted) can be used to compensate for these aperture discontinuities with two deformable mirrors and enhanced the coronagraphic performance. Thanks to these recent progress, the selected concepts for WFIRST-AFTA are expected to reach 10^9 contrast over a 10% bandpass at moderate inner working angle ($3\,\lambda_0/D$) with the WFIRST-AFTA pupil (Trauger et al. 2013; Guyon et al. 2014; Zimmerman et al. submitted) after image post-processing (Debes et al. submitted; Ygouf et al. 2015).

The Apodized Pupil Lyot Coronagraph (APLC Aime et al. 2002; Soummer et al. 2003a; Soummer 2005; Soummer et al. 2009, 2011) is one of the leading type of coronagraph in the current-generation ground-based instruments; it is used in the Gemini Planet Imager (GPI), Very Large Telescope (VLT) SPHERE, and Palomar P1640 (Macintosh et al. 2014; Beuzit et al. 2008; Hinkley et al. 2011). For example, the GPI APLC is designed to reach a raw contrast of 10^7 at 0.2 arcsec in 20% broadband light, and in the presence of central obstructions and support structures. It uses a prolate apodization, which derives from the eigenvalue problem associated with the Lyot-style coronagraphic propagation for a given mask size. The design was optimized for the contrast as metric, by adjusting the prolate function (eigenfunction) and Lyot stop geometry to establish quasi-achromatic solutions (Soummer et al. 2011). However, since there is only a single degree of freedom in the definition of the apodizer (the eigenvalue of the problem), the raw performance is limited to the 10^7 to 10^8 contrast range.

We have recently generalized the APLC design by using a shaped pupil optimization approach (Kasdin et al. 2003; Vanderbei et al. 2003; Carlotti et al. 2011) to develop broadband solutions with raw contrast up to 10^{10} in one dimension (Pueyo & Norman 2013; N'Diaye et al. 2015a). In addition, we have also identified solutions with this approach that increase robustness to telescope pointing errors, focus drifts and vibrations or stellar angular size. This is achieved by producing a point spread function (PSF) core smaller than the projected coronagraphic mask, allowing movement of the star PSF within the mask with virtually no impact on the coronagraph performance (N'Diaye et al. 2015a). In N'Diaye et al. (2015a), we established the case for circular axi-symmetric obstructed pupils, using one-dimensional optimization. In that case, additional features in the pupil (e.g. support structure) deteriorate the contrast in the exoplanet search area. These effects can be partially mitigated by readjusting the Lyot stop geometry Sivaramakrishnan & Yaitskova (2005); Sivaramakrishnan & Lloyd (2005); Soummer et al. (2009), but this approach is limited to contrast up to $\sim 10^8$.

In this paper we generalize the approach and derive new solutions for telescope apertures with arbitrary features (central obstruction, spiders, segmentation) by extending our approach from one to two-dimension (2D) pupil optimization. We present new APLCs using shaped-pupil (SP) type apodizations. These hybrid APLC/SP coronagraphs are manufacturable with current mask technologies (Balasubramanian et al. 2013). Carlotti et al. (in prep.) has recently proposed to combine standalone optimized shaped pupils and Lyot coronagraphs. Based on this approach, Zimmerman et al. (submitted) recently proposed a design for the WFIRST-AFTA coronagraphic instrument to obtain a 10^9 raw contrast level. In our approach, we optimize the SP apodization for the whole APLC propagation, including SP apodizer, focal plane mask, Lyot stop and final image with coronagraphic dark zone. As an application, we propose a design to produce a 10^{10} raw contrast with a segmented telescope aperture.

After detailing the APLC/SP optimization methodology and our design example, we analyze the robustness of our solution to stellar angular size and derive lower space observation bounds for nearby stars with our concept. We finally estimate and discuss the yield of Earth-like planet candidates with our concept for a future mission with different telescope aperture sizes. Contrast can be assessed in many different ways, as recently recalled by Mawet et al. (2014). In this paper and unless otherwise stated, we will refer to the raw contrast and quantify it as the averaged residual intensity over a given image area and normalized by the stellar peak intensity.

2. PRINCIPLE OF HYBRID APLC/SHAPED PUPIL CORONAGRAPH

2.1. *Formalism of Coronagraphy with Apodization*

We briefly recall the chromatic formalism of the Lyot-style coronagraph with apodization, following the notations of Aime et al. (2002) and Soummer et al. (2003a,b), for a given wavelength λ within the bandpass $\Delta\lambda$ centered at the wavelength λ_0. The vectors $\boldsymbol{r}$ and $\boldsymbol{\xi}$ (of modulus r and ξ) denote the two-dimensional position vectors in the pupil and focal planes.

The coronagraph setup involves four successive planes (A, B, C, D) in which A defines the entrance pupil $P = P_0\,\Phi$ that combines the telescope pupil shape P_0 and the apodization Φ, B sets the location of a hard-edged focal plane mask (FPM) of diameter m and transmission $1 - M$ with $M(\boldsymbol{\xi}) = 1$ for $\xi < m/2$ and 0 otherwise, C includes the Lyot stop L to filter out the diffraction due to the FPM, and D represents the final image plane. The optical layout of the coronagraph is such that the complex amplitudes of the electric field in two successive planes are related by a Fourier transform. We call $\hat{f}$ the Fourier transform of the function f. In the absence of magnification, the electric field amplitude in the four successive planes writes as follows:

$$\Psi_A(\boldsymbol{r},\lambda) = P(\boldsymbol{r}) \tag{1a}$$

$$\Psi_B(\boldsymbol{\xi},\lambda) = \frac{\lambda_0}{\lambda}\widehat{\Psi}_A\left(\frac{\lambda_0}{\lambda}\boldsymbol{\xi},\lambda\right)(1 - M(\boldsymbol{\xi})) \tag{1b}$$

$$\Psi_C(\boldsymbol{r},\lambda) = \left(\Psi_A(\boldsymbol{r},\lambda) - \Psi_A(\boldsymbol{r},\lambda) * \frac{\lambda_0}{\lambda}\widehat{M}\left(\frac{\lambda_0}{\lambda}\boldsymbol{r},\lambda\right)\right)L(\boldsymbol{r}) \tag{1c}$$

$$\Psi_D(\boldsymbol{\xi},\lambda) = \left(\frac{\lambda_0}{\lambda}\right)^2\left(\widehat{\Psi}_A\left(\frac{\lambda_0}{\lambda}\boldsymbol{\xi},\lambda\right)(1 - M(\boldsymbol{\xi}))\right) * \widehat{L}\left(\frac{\lambda_0}{\lambda}\boldsymbol{\xi},\lambda\right) \tag{1d}$$

where $*$ symbolizes the convolution operator. In the absence of FPM, the electric field amplitude in the final image plane

is simply given by:

$$\Psi_D^0(\boldsymbol{\xi},\lambda) = \left(\frac{\lambda_0}{\lambda}\right)^2 \widehat{\Psi}_A\left(\frac{\lambda_0}{\lambda}\boldsymbol{\xi},\lambda\right) * \widehat{L}\left(\frac{\lambda_0}{\lambda}\boldsymbol{\xi},\lambda\right) \tag{2}$$

Assuming a flat stellar spectrum, the coronagraphic image intensity over the bandpass $\Delta\lambda$ can be deduced from Equation (1d) by means of an operator $\mathcal{I}_{\Delta\lambda}$ as

$$\mathcal{I}_{\Delta\lambda}[\Phi(\boldsymbol{r})](\boldsymbol{\xi}) = \frac{1}{\Delta\lambda}\int_{\Lambda} |\Psi_D(\boldsymbol{\xi},\lambda)|^2 \, d\lambda\,, \tag{3}$$

where Λ defines a set of wavelengths λ such that $|\lambda - \lambda_0| < \Delta\lambda/2$.

The analysis of the re-imaged pupil plane offers insights on the coronagraph behavior. According to Equation (1c), perfect starlight suppression is obtained if the direct wave (entrance pupil amplitude) and the wave diffracted by the FPM (convolution integral) matches within the Lyot stop. Different approaches have been considered to obtain a perfect subtraction between these two waves. A first approach consists of modifying the geometry of the mask to obtain perfect subtraction within a reduced area of the pupil. Such strategy corresponds to the band-limited mask coronagraph (Kuchner & Traub 2002). We follow a second approach seeking for a modification of the entrance pupil amplitude by means of the apodization Φ to match the two waves within the re-imaged pupil (Aime et al. 2002; Soummer et al. 2003a).

The existence of a perfect extinction solution for the Roddier phase mask coronagraph (Roddier & Roddier 1997) in monochromatic light was numerically derived by Guyon & Roddier (2000) and analytically showed by Aime et al. (2002) and Soummer et al. (2003a). For the APLC, there is no solution for complete starlight suppression but Aime et al. (2002) and Soummer et al. (2003a) analytically show that prolate apodization solutions nearly achieve complete starlight removal with circular and rectangular unobstructed apertures. These solutions have been generalized to the obstructed circular aperture (Soummer 2005) and the arbitrary non circular aperture in the context of Extremely Large Telescopes (ELTs, Soummer et al. 2009; Martinez et al. 2007). These solutions for opaque masks have also been extended to the complex amplitude FPMs for small IWA coronagraphy (Guyon et al. 2010a, 2014).

In the case of opaque FPM, Soummer et al. (2011) studied the chromatic properties of APLC using prolate apodizers and found the existence of quasi-achromatic solutions over large bandpasses. They derive a continuous family of prolate apodizations corresponding to the telescope geometry and select the optimal set of apodization and Lyot stop geometry using contrast in the final image plane within the controllable adaptive optics (AO) area as an optimization metric to obtain the broadband APLC designs that are currently implemented in P1640 and GPI (Hinkley et al. 2011; Macintosh et al. 2014).

The raw performance of the current implementations are however limited by the available degrees of freedom (apodization and Lyot stop geometry) in the optimization approach. We recently found new functioning modes for the APLC by proposing an alternative approach based on the shaped-pupil like optimization to design Lyot-style coronagraph with improved performance in terms of contrast and inner working angle (Pueyo & Norman 2013; N'Diaye et al. 2015a). In N'Diaye et al. (2015a), we propose broadband solutions for centrally obstructed circular apertures, using 1D pupil optimization. We here show the existence of solutions for arbitrary apertures with pupil features such as segmentation and spiders by exploiting our approach to 2D pupil.

2.2. *Numerical Optimization for the Apodizer*

We define a numerical optimization problem with Lyot-style coronagraph that includes the aperture, FPM, and Lyot Stop geometries, and constraints on the coronagraphic intensity in a given focal plane region (dark zone) and we look for apodization solutions for the APLC. Among these solutions, we seek for the apodization with the best throughput in an attempt to maximize the number of photons from companions around the observed star during observing time. Following the classical shaped-pupil type optimization problems (Vanderbei et al. 2003; Kasdin et al. 2003; Carlotti et al. 2011), the optimal pupil apodization for APLC can be found by solving the following optimization problem:

$$\max\left[\int_{P_0} \Phi(\boldsymbol{r})d\boldsymbol{r}\right] \quad \text{under the contraints:} \tag{4a}$$

$$|\Psi_D(\boldsymbol{\xi},\lambda)|^2 < 10^{-C}\left|\Psi_D^0(\boldsymbol{0},\lambda_0)\right|^2 \quad \text{for} \quad \begin{cases}\rho_i < \xi < \rho_o \\ |\lambda-\lambda_0| < \Delta\lambda/2\end{cases} \tag{4b}$$

$$0 \le \Phi(\boldsymbol{r}) \le 1, \tag{4c}$$

where the significance of each line is further explained below:

(4a) The apodizer throughput is a quadratic function of the field amplitude. Assuming positive, real-valued apodization amplitude (see Eq. (4c)), we use this linear function of the field amplitude as a proxy to maximize the apodizer throughput over the area defined by the initial aperture shape P_0.

(4b) The coronagraphic image intensity is constrained at all the wavelengths over the bandpass to achieve a contrast 10^C over the area $\mathcal{D}$ in broadband light. This region is defined between its inner and outer edges, respectively ρ_i and ρ_o.

(4c) The transmission of the amplitude apodization is real, positive and normalized.

N'Diaye et al. (2015a) set constraints on the apodizer derivative to obtain continuous solutions with limited oscillations within the pupil apodization and avoid bang-bang solutions. The problem was written in one dimension with linear constraints, allowing resolution with a linear programming solver (Vanderbei 2009)

The 2D problem does not include constraints on the apodizer derivative, thus enabling binary apodization solutions using shaped-pupil manufacturing technologies. While the 2D optimization problem can also be expressed linearly as the 1-Dimensional problem, we find that this problem in AMPL language (Fourer et al. 1990) with the solver Gurobi (Gurobi Optimization 2015) is handled slightly more effectively using the image intensity instead of the field as showed in Eq. (4b) from described above. This somewhat counter-intuitive behavior is likely to be solely due to technical implementation of these various solvers.

The computation of the coronagraphic electric field for the APLC requires three successive Fourier transforms (FT) between the electric field amplitude in the four successive planes of the optical layout. We adopt the semi-analytical approach from Soummer et al. (2007) for fast Lyot-style coronagraph computation with simultaneous highly sampled pupils and focal plane masks. The semi-analytical and FFTs approaches are strictly equivalent in the absence of field of view limitations in the FPM plane. Further error budget studies should provide the acceptable size of the mirror for a reflective FPM

to obtain a compatible 10^{10} contrast level. We also express the Fourier transforms (FTs) involved in the coronagraphic electric field calculation using discrete Riemann sum in Cartesian coordinates. Following Vanderbei (2012), these 2D FTs are performed in two steps with a separation of the variables to reduce the problem complexity. Carlotti et al. (2011) successfully applied this strategy to design shaped pupils in a two-plane configuration that simply involves a single FT for the coronagraphic electric field computation.

We here seek solutions based on an apodizer and focal plane mask with real amplitude transmission (no phase terms). Further solutions with complex amplitude apodizer and focal plane masks could also be investigated based on the optimization problem set above without loss of generality, but this study is out of the scope of this paper.

3. APPLICATION TO A LARGE SEGMENTED APERTURE

3.1. *Solution*

To illustrate these new APLC/SP hybrid solutions, we present a design optimization for a 37-hexagonal-segment telescope aperture with central obstruction and spiders, such as one of the envisioned design for the ATLAST mission concept (Postman et al. 2012) or the geometry corresponding to existing ground-based telescopes W.M. Keck, or Gran Telescopio Canarias. In the following, all the pupil geometry parameters (obstruction, spiders, gaps) are expressed in aperture diameter ratio.

We assume an inscribed circular aperture over the 37 segments, with 20% central obstruction, 1% spiders and 0.2% segments gaps, see Figure 1 top left. For the coronagraph design, we consider an FPM of radius $m/2 = 4\,\lambda_0/D$. The contrast target is set to 10^{10} in a focal plane region $\mathcal{D}$ delimited by inner and outer edge radii of ρ_i =3.5 and ρ_o =20.0 λ_0/D. Following the approach developed in N'Diaye et al. (2015a), we set the dark zone inner edge with a smaller radius than the FPM. Such resulting designs do not allow observations of companions at separations smaller than the projected FPM angular size but the coronagraphic solution will present a reduced sensitivity to low-order aberrations, such as telescope jitter and thermal or mechanical focus drift, as well as a reduced sensitivity to the stellar diameter.

We finally consider a circular Lyot stop with the same outer size as the entrance aperture, with 40% central obstruction and 2% spiders, corresponding to an oversizing factor of 2 with respect to the entrance pupil characteristics, but without reticula for the segment gaps (no obstruction for these aperture discontinuities), see Figure 1 middle left. To achieve a broadband APLC design, we run an optimization with constraints at three wavelengths that are centered around λ_0 and equally spatially sampled one to another over 10% bandwidth. Note that while only three wavelengths are used in this case for the optimizer, the broadband profiles illustrated in the figures include 11 simulated wavelengths. The parameters are summarized in Table 1.

With these parameters, we solve our optimization problem and find an APLC design solution with the shaped-pupil apodization displayed in Figure 1 top right, leading to a 28% total coronagraph throughput. Our solution produces the relayed pupil image that is showed at λ_0 before and after the Lyot stop application in the middle right and bottom left frames. As expected, most of the star diffracted light is found at the aperture discontinuities (Sivaramakrishnan & Yaitskova 2005; Sivaramakrishnan & Lloyd 2005) and constrained within the area blocked by the Lyot stop geometry, allowing an efficient starlight rejection by the Lyot Stop. It is interesting to note that the introduction of a Lyot stop reticula (Sivaramakrishnan & Yaitskova 2005; Sivaramakrishnan & Lloyd 2005) in this specific design is counterproductive in terms of starlight suppression: it results in additional diffracted light within the final image plane and a deterioration of the contrast in the dark region. An APLC solution using a Lyot stop with reticula can be designed with our approach if the geometry of the diaphragm is included in the optimization process.

The broadband coronagraphic image and its corresponding averaged intensity profile are displayed in Figures 1 bottom right and 2 for designs with three different dark zone outer bound, illustrating the ability of our approach to design APLCs that could produce broadband PSFs with 10^{10} dark region in the presence of an arbitrary aperture.

TABLE 1
PARAMETERS FOR THE DESIGN SHOWED IN FIGURE 1.

parameters	value
Contrast C	10^{10}
Dark zone inner edge radius ρ_i	3.5 λ_0/D
Dark zone outer edge radius ρ_o	20.0 λ_0/D
focal plane mask radius $m/2$	4.0 λ_0/D
Aperture	20% central obstruction
	1% aperure size spiders
	0.2% aperture size gaps
Lyot stop	40% central obstruction
	2% aperutre size spiders
	no segmentation
Broadband optimization	3 wavelengths within 10% band
Broadband PSF profiles calculations	11 wavelengths within 10% band

3.2. *Apodizer Manufacturing Aspects*

Because of numerical limitations for the number of points in the pupil, our APLC/SP optimization produces an apodization which values are mostly black or white (37% of the apodization points have a 0 or 100% amplitude transmission level to a 1% precision) but that also contains gray points. We investigated the conversion of these apodization solutions into binary apodizers that can be manufactured using the current state-of-the-art technologies developed for shaped pupil apodizers (Balasubramanian et al. 2013).

Our grey designs are obtained with a 600-point diameter. A pupil sampling increase or a full exploration of the coronagraph parameter space (FPM size, Lyot stop geometry, dark zone dimensions) could allow us to find fully black and white designs but proves computationally challenging. Instead, we investigated new versions of our original grey design, using different methods to convert our grey pixels into black and white, such as simple rounding of the values or a sub-pixelization of the gray design pixels followed by application of the error diffusion algorithm (EDA, Floyd & Steinberg 1976), a process that has been used for the manufacturing of grey apodizers for GPI, SPHERE and P1640 to reach 10^6–10^7 raw contrast levels (Dorrer & Zuegel 2007; Martinez et al. 2009; Sivaramakrishnan et al. 2009). At 10^{10} raw contrast levels, the same process is expected to be efficient if the performance of the binary design is validated numerically and then experimentally and as long as the pixel size of the apodizer prototype remains significantly larger than the wavelength of

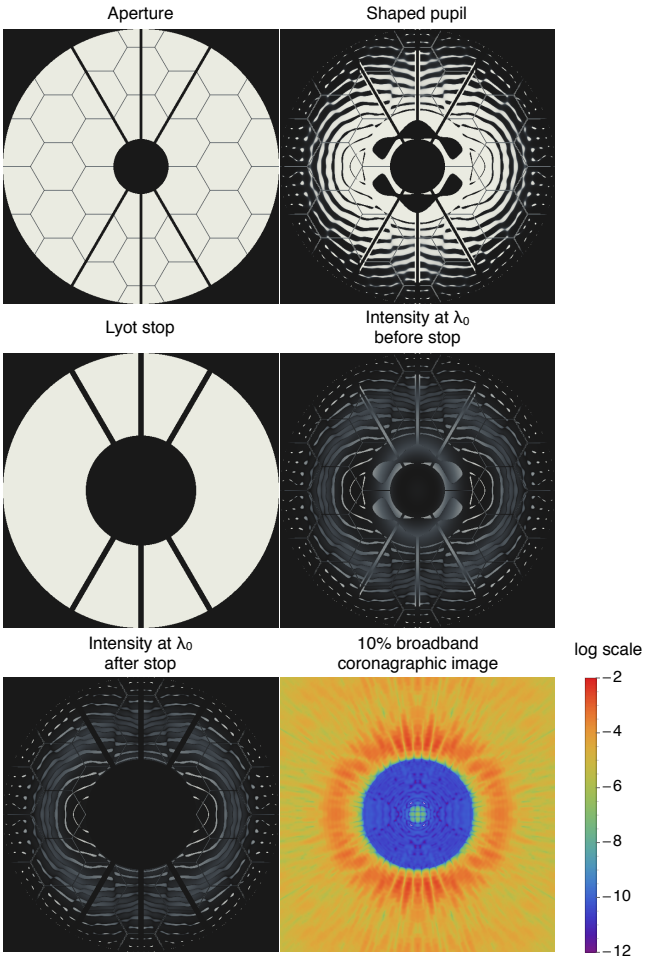

FIG. 1.— Top left: telescope aperture. Top right: Shaped pupil apodization for the APLC with the previous aperture. Middle Left: Lyot stop shape. Middle right and bottom left: Residual intensity in the relayed pupil plane before and after Lyot stop application. Bottom right: Broadband coronagraphic image of the star with the APLC/shaped pupil hybrid design using the shaped pupil and Lyot stop showed above, and the FPM of radius $r = 4\,\lambda_0/D$. A 10^{10} contrast region with 3.5 λ/D inner and 20 λ_0/D outer edges is achieved with our solution over a 10% spectral bandpass, paving the way for the direct imaging of Earth twins with future large missions.

observation.

Figure 3 displays the contrast curves for our coronagraph design with a dark zone outer edge ρ_1=10 λ_0/D using the original apodizer from the optimizer and its binarized versions from numerical simulations. A contrast loss of two orders of magnitude is observed by simply rounding the pixel values. The contrast loss can be recovered by using the EDA method and sufficient oversampling. With a factor of 16 for the sub-pixelization, we almost recover the initial 10^{10} contrast level reached with our optimized design. With this 9600-pixel diameter apodizer, we translate these values into physical units for manufacturing considerations. We assume the use of black silicon technologies with the current state-of-the-art for the fabrication of a reflective apodizer prototype (Balasubramanian et al. 2013). Assuming a 10 μm pixel size, an apodizer prototype with 96 mm diameter can be manufactured fulfilling the specifications that enable the starlight suppression down to 10^{-10} intensity level in visible light with a telescope segmented aperture. This result shows the existence of suitable, broadband diffraction suppression solutions with already manufacturable components (shaped-pupil apodization,

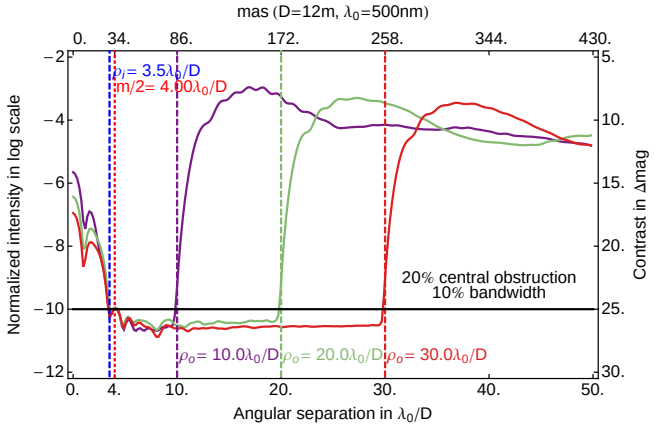

FIG. 2.— Azimuth averaged intensity profile of the coronagraphic image produced by our APLC/SP hybrid solutions in 10% broadband light with the components showed in Figure 1, for three different dark zone outer edges. The vertical dashed lines represent the bounds of the search area $\mathcal{D}$ (ρ_i = 3.5 λ_0/D [blue] and ρ_o =10.0, 20.0, and 30.0 λ_0/D [purple, green, red]). The red dot line delimits the FPM radius, set to $m/2$ =4 λ_0/D. The averaged contrast over the spectral band in the dark region is below 10^{-10} (black horizontal line). For each dark zone outer bound, the coronagraph has here been designed to produce an image core smaller than the projected FPM size, allowing for both enlargement and expansion of the PSF without impact on the contrast, making this design virtually insensitive to low-order aberration, as explained in N'Diaye et al. (2015a).

FPM, Lyot stop) for the direct imaging and spectral analysis of Earth twins with large segmented apertures. Further coronagraph designs using binary apodization with a smaller sampling are currently under investigation to reduce the pupil dimensions in the context of a coronagraph instrument.

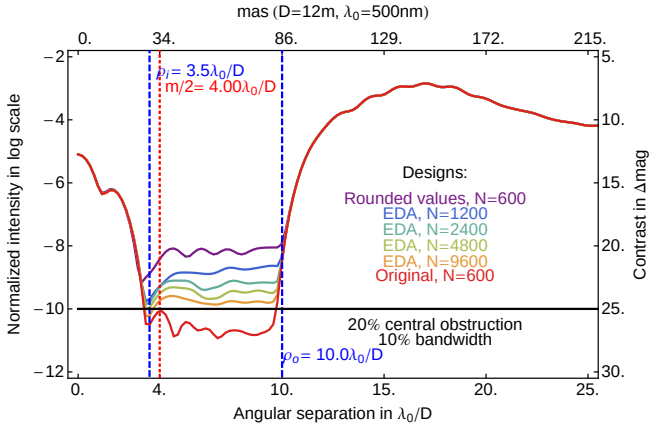

FIG. 3.— Azimuth averaged intensity profile of the coronagraphic image reached by an APLC solution in 10% broadband light and the parameters shown in Table 1, except for the Lyot stop which presents a 36% instead of 40% obstruction, providing a quasi-binary shaped pupil. Profiles are represented for the design with the original grey version, rounded values version, and the binarized versions using error diffusion algorithm (EDA, see e.g. Dorrer & Zuegel (2007)) with different lateral size N obtained by sub-pixelization of the original design gray pixels. The dashed blue vertical lines delimit the high-contrast search area $\mathcal{D}$ (ρ_i = 3.5 λ_0/D and ρ_o =10.0 λ_0/D). The red dot line delimits the FPM radius, set to $m/2$ = 4 λ_0/D. The averaged contrast over the spectral band in the dark region is below 10^{-10} (black horizontal line). The 10^{10} contrast performance of the original design is almost recovered with a EDA version using N=9600. Relating on current black silicon technologies to manufacture Shaped pupil mask for WFIRST-AFTA coronagraph (Balasubramanian et al. 2013), we translate these values into physical units. Assuming a 10 μm size for a pixel, the apodizer of our design can currently be fabricated with a 96 mm diameter prototype to work in visible light.

3.3. *Off-axis throughput*

Beyond starlight removal, estimating the amount of photons from the nearby objects through the coronagraph is important to determine the observation time required for accurate photometry, astrometry, and spectral analysis of the star companions. We consider the Airy throughput as a metric to determine the fraction of transmitted light from off-axis companions through our coronagraphic system. The Airy throughput is defined as the ratio of the total energy inside the core of the off-axis coronagraphic PSF to the total energy inside the core of the telescope PSF. Since our design makes use of a pupil apodization, the image of an off-axis companion is an apodized PSF, which sharpness is defined by the shaped pupil. Throughputs are displayed for our coronagraph designs with three different PSF dark zones in Table 2. For the Airy throughput, we adopt a $0.75\,\lambda_0/D$ core radius for the photometric aperture to account for the modified light distribution in the PSF in the presence of the shaped-pupil apodization. This ideal value has been determined after calculating the exo-Earth yield, presented in the next section, as a function of the photometric size aperture to maximize the planet's light signal compared with different sources of noise backgrounds (leaked starlight, exozodi, local zodi, etc.). In the background-limited regime, for an Airy pattern PSF, the ideal photometric aperture radius is $\sim 0.7\,\lambda_0$/D, which contains $\sim 70\%$ of the planet's PSF.

Our throughputs have been estimated with a sampling of 5 pixels per resolution element (λ_0/D). For the design showed in Figure 1, the Airy throughput within the dark region and with respect to the segmented aperture is estimated with a maximum of 18.4% and with about half of it at an angular separation of $4.2\,\lambda_0/D$, giving the IWA of our design. Table 2 summarizes the throughputs for our coronagraph designs, showing its evolution as a function of different separations.

Further improvements in contrast and IWA are expected with a full exploration of the parameter space for this coronagraph (FPM, Lyot stop geometry, bandwidth), following N'Diaye et al. (2015a), to identify the solution with the best throughput for a given aperture geometry.

TABLE 2
THROUGHPUT ESTIMATES FOR OUR CORONAGRAPH DESIGNS IN FIGURE 2 WITH DIFFERENT DARK ZONE OUTER BOUNDS. AIRY THROUGHPUTS ARE ESTIMATED WITH A $1.5\,\lambda_0/D$ SIZE PHOTOMETRIC APERTURE , USING 5 PIXELS PER λ_0/D.

Values wrt to aperture geometry		Clear			Segmented		
ρ_o in λ_0/D		10.0	20.0	30.0	10.0	20.0	30.0
Airy throughput in % at	$4.0\,\lambda_0/D$	3.1	2.9	2.7	5.8	5.4	5.1
	$4.2\,\lambda_0/D$	5.1	4.7	4.5	9.5	8.9	8.4
	$5.0\,\lambda_0/D$	8.6	8.1	7.7	16.1	15.2	14.4
	$6.0\,\lambda_0/D$	10.0	9.3	8.8	18.7	17.5	16.5
Max. Airy Throughput in %		10.5	9.8	9.3	19.8	18.4	17.4

3.4. *Stellar Angular Size Sensitivity Analysis*

Since on-axis resolved stars is identified as one of the major concerns for high-contrast imaging of extrasolar planets with future large telescopes (Guyon et al. 2006), we analyze the impact of the stellar angular size on the performance of our coronagraphs.

An on-axis resolved star can be seen as a combination of off-axis point sources at all the angular positions ranging up to the stellar angular radius. This is equivalent to consider a sum of tip-tilt point sources weighted by $2\pi\xi$ where ξ here corresponds to the offset position. We can devise the coronagraph contrast sensitivity at $5\,\lambda_0$/D by averaging the solid-line profiles for the coronagraphic images of tip-tilt sources with weights corresponding to the offset positions, as previously done in N'Diaye et al. (2015a).

Figure 4 shows the contrast performance at $5\,\lambda_0$/D of the $20\,\lambda_0/D$-OWA design as a function of the angular size of the observed objects. Our designs are robust enough to stellar angular size to allow observation of planets around Sun-like stars located beyond 4.4 pc.

With our hybrid concept and assuming a perfect and stable wavefront, a solar system twin with unresolved companions at 13.5 pc could be observed with a 12 m telescope in 8 h and characterized with less than two-day exposure time under photon-noise limited regime, see Figure 5. In this numerical simulation, we did not account for the motion of the planet and the required post-processing methods to increase the signal-to-noise ratio of planets in such long period observations. Promising strategies for such effect have recently been proposed to efficiently combine the different frames of the sequence of observation for the planet with orbital motion during the observations (Males et al. 2015). Our design is fully functioning for detection and characterization of Earth twins around nearby stars.

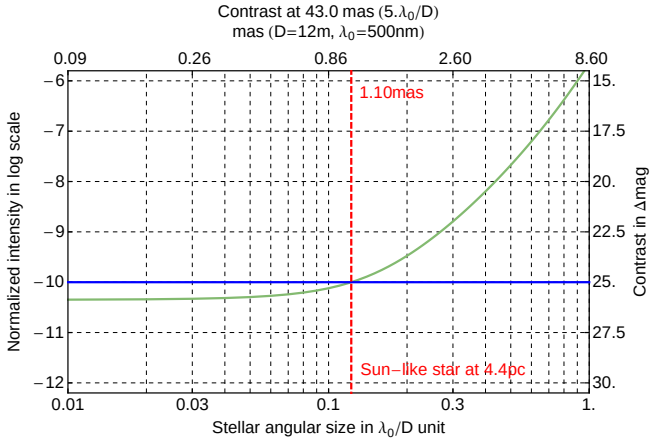

FIG. 4.— Averaged intensity of the broadband coronagraphic image at a $5\,\lambda_0/D$ angular separation from the optical axis as a function of the stellar angular size. The curve is obtained for our design with ρ_1 =$20\,\lambda_0/D$. Blue solid line denotes the 10^{-10} intensity level. Our design presents a plateau and intensity levels below 10^{-10} for stellar angular size up to $0.12\,\lambda_0/D$, underlining the contrast performance stability of our coronagraph design. Assuming a 12 m telescope at 500 nm, our coronagraph is robust to stellar angular sizes up to 1.1 mas, allowing observations of planets around Sun-like star located beyond 4.4 pc.

4. EXO-EARTH YIELD ESTIMATE

The number of observable Earth-sized planets in the habitable zone of their parent star (exo-Earth candidates) represents a key metric for future exoplanet imaging missions. Several studies have estimated the exo-Earth candidate yield with future coronagraphic missions (e.g. Brown 2005; Brown & Soummer 2010). We estimate the exo-Earth candidate yield for a future exoplanet direct imaging mission with our coronagraph design using the methods developed by Stark et al. (2014) and Stark et al. (2015). These methods maximize the yield of Earth twins by simultaneously optimizing many aspects of the observation plan, including the exposure times of all observations, the number of visits to each star, and the delay time between revisits.

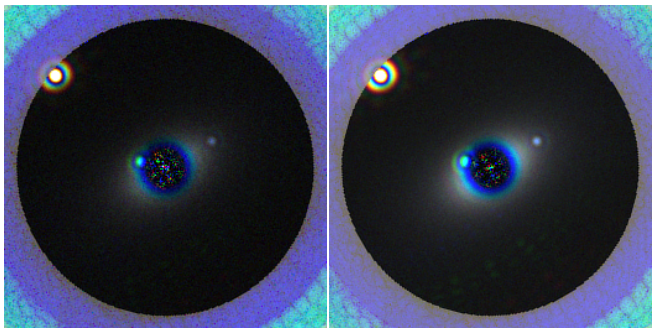

FIG. 5.— Simulated multicolor pictures of a solar system twin at 13.5 pc with a 12 m telescope and our coronagraph design with an OWA ρ_1 =30 λ_0/D at different exposure times (from left to right: 8h, 40h). The solar system was modeled with the Haystacks project (Courtesy A. Roberge et al.), including spectroscopic and spatial information for all the components within the exoplanetary system. Each picture is a composite of three images on three channels around 400, 500 and 600 nm, each with 10% bandpass and a coronagraph optimized for this band. In this simulation, we assume a perfect wavefront, no wavefront drifts between the target solar system star and calibrator star for the image processing, and only photon noise. Earth is at 2 o'clock and is indeed blue, Venus is at 9 o'clock, Zodiacal light is elongated along the 2-8 o'clock direction, Jupiter is at 10 o'clock in the red channel (600 nm): it is outside of the dark hole at shorter wavelengths. In that channel, most of Venus is hidden by the coronagraph. Linear and logarithmic scale representations are used inside and outside the high-contrast region for each coronagraph.

For our design reference missions analysis, we assume a five-year mission using our coronagraph design with two years dedicated to exo-Earth detection (one total year of exposure time and another year of overheads). We assume the dimmest detectable planet is 27.5 mag fainter than its host star, one order of magnitude beyond the raw contrast. We note that although our adopted noise floor is very optimistic, noise floors beyond ~26 mag do not greatly impact the yield; adopting a more conservative noise floor of 26 mag fainter than the host star will not change our results significantly (Stark et al. 2015). We assume an observation time only devoted to detection in V band (no spectral characterization) with signal-to-noise ratio SNR≥7, and noiseless detectors (photon noise limited observations).

We use several astrophysical assumptions to estimate our Earth-analog candidate yield, see Stark et al. (2015) for a detailed description of astrophysical assumptions made here. We assume Earth twins with parameters as described in Stark et al. (2014). We adopt the optimistic habitable zone definition from Kopparapu (2013) for Sun-like stars (OKHZ), ranging from 0.75 - 1.77 AU, and scale it with the square root of the stellar luminosity. Exo-Earth orbits are assumed circular, based on the eccentricity-radius correlation from Kane et al. (2012). We assume $\eta_\oplus$ = 0.1, the fraction of stars with Earth-sized planets in the OKHZ, based on planet occurrence estimates ranging from 0.05 to 0.2 for Sun-like stars (Petigura et al. 2013; Marcy et al. 2014; Silburt et al. 2015). In this simulation, we also include different amounts of exozodiacal dust in units of zodis, using the "zodi" definition from Stark et al. (2014).

Figure 6 represents the yield of exo-Earth candidates as a function of the telescope diameter for different exozodi levels. The yield for a mission equipped with our coronagraph improves substantially as the telescope diameter increases. Assuming a future constraint on the median exozodi level of <3 zodis, we estimate our coronagraph design with a 12 m segmented aperture can detect 12.5 exo-Earth candidates, assuming a perfect and stable wavefront.

Clearly, our novel design here produces a moderate yield for such large telescope. However, we have here presented a 10^{10} raw contrast design as a first iteration, representing a proof of existence of coronagraphs that can both be manufactured as of today and handle large segmented aperture in terms of starlight attenuation for Earth twin observations. This preliminary design leaves room for yield improvement in coronagraphy, in particular with the APLC/SP hybrid concept, by exploring trade-offs in coronagraph design parameters (focal plane mask size and type, inner and outer edges of the dark zone, Lyot stop geometry).

In an attempt to identify the key points for yield enhancement, we assess the impact of the coronagraph parameters on the yield, see Table 3. A few observations can be derived from its analysis:

1. the dark region outer edge is a good parameter to degrade in coronagraph design since it barely alters the exo-Earth yield and its reduction allow increasing the amount of flux in the PSF core. In contrast, maintaining a large dark region outer edge would favor the detection of companions, such as mature Jupiter-like planets at large separations

2. trading off contrast for IWA is worthwhile if we gain a $> 0.5\,\lambda_0/D$ in IWA for a factor of 2 degradation in contrast

3. the PSF core size impacts our design performance

4. since we estimate contrast with respect to the PSF peak in the absence of focal plane mask, the throughput does not affect the amount of leaked starlight hitting the detector. Thus, increasing the throughput is more valuable than enlarging the bandwidth or mission lifetime because it does not increase one of the sources of noise.

These remarks give us a clear path for further coronagraph designs to enhance the yield and provide a maximized science return with future large space observatories.

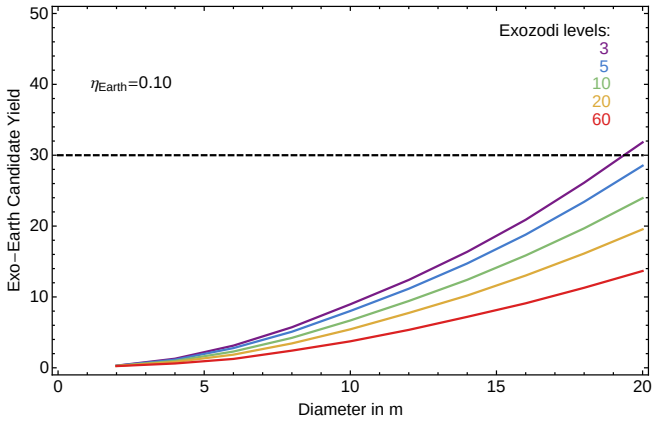

FIG. 6.— ExoEarth candidate Yield with our coronagraph design as a function of the telescope diameter for different exozodi levels. Following the 12 m telescope scenario for the ATLAST concept, we find 12.5 detectable exo-Earth candidates within 3 zodi levels for this mission with our coronagraph characteristics (IWA, OWA, contrast, Airy throughput), assuming a perfect and stable wavefront. Unsurprisingly, the exoplanet number drops at 5 with 60 exo-zodi levels but the initial exo-Earth yield is recovered by increasing the aperture size up to 20 m.

TABLE 3
IMPACT OF CORONAGRAPH PARAMETERS ON EXO-EARTH YIELD, ASSUMING A 10 M TELESCOPE WITH 3 ZODIS OF EXOZODI. IN THIS PARAMETRIC STUDY, THE APODIZER HAS NOT BEEN RE-OPTIMIZED FOR EACH SET OF PARAMETERS.

Parameter	Change	Exo-Earths number change
IWA	-0.5 λ_0/D	+1.1
	+0.5 λ_0/D	-1.0
OWA	-2.0 λ_0/D	-0.1
	+2.0 λ_0/D	+0.1
Contrast	x 0.5	-1.7
	x 2.0	+1.0
Bandwidth	x 0.5	-2.7
	x 2.0	+3.3
Throughput	x 0.5	-4.0
	x 2.0	+4.7
PSF radial size	x 0.5	+6.4
	x 2.0	-4.7
Total exposure time	x 0.5	-2.7
	x 2.0	+3.3

5. CONCLUSION

We have proposed new APLC/shaped pupil hybrid solutions suitable for arbitrary telescope apertures including central obstruction, segmentation, and spiders. These new solutions are particularly interesting since they are already manufacturable, by building directly on shaped-pupil technology.

To illustrate our new APLC solutions, we have presented a diffraction suppression system that could handle on-axis telescope with pupil features for broadband observations with 10^{10} contrast and that is virtual insensitivity to low-order aberrations and star diameter. In this example, a maximum Airy throughput of 18% is achieved to detect the photons from off-axis companions through our coronagraph design.

We have presented our approach with an APLC solution as a simple illustration of the concept. Further improvements are expected with an exploration of the parameter space that includes FPM diameter, Lyot stop feature sizes, dark zone dimensions, and spectral bandwidth to find coronagraph solutions with a maximized number of off-axis companion photons for a given integration time. Also, we have not explored yet different telescope geometries that still have degrees of freedom e.g. obstruction ratio, width of support structures. We can also imagine an optimal combination of our hybrid APLC/SP solutions with the Active Combination of Aperture Discontinuities (ACAD, Pueyo & Norman 2013; Mazoyer et al. submitted) for diffraction control with arbitrary apertures in particular as a way to improve the off-axis companion throughput. Our approach presented in the context of APLC can be applied to vector vortex coronagraphs (Mawet et al. 2005) and dual-zone phase mask coronagraphs (Soummer et al. 2003b; N'Diaye et al. 2012), or other complex masks (Guyon et al. 2010a) to provide solutions with 10^{10} contrast at very small IWA ($< 2\,\lambda_0/D$).

A comparison of the derived solutions in terms of exo-Earth yield estimate can be made to find the coronagraph design that maximizes the number of observable targets for a given mission. Such studies will be helpful to prepare future Design Reference Missions.

The authors are grateful to the referee for the insightful suggestions and comments on the manuscript. This work is supported by the National Aeronautics and Space Administration under Grant NNX12AG05G and NNX14AD33G issued through the Astrophysics Research and Analysis (APRA) program (PI: R. Soummer). This material is also partially based upon work carried out under subcontract 1496556 with the Jet Propulsion Laboratory funded by NASA and administered by the California Institute of Technology. The authors would like to thank A. J. E. Riggs, N. Zimmerman, N. J. Kasdin, and R. Vanderbei for helpful discussions on shaped pupil designs and modeling. The authors also warmly acknowledge Aki Roberge and his team for Haystacks model of the solar system.

REFERENCES

Aime, C., Soummer, R., & Ferrari, A. 2002, A&A, 389, 334
Balasubramanian, K. 2008, Appl. Opt., 47, 116
Balasubramanian, K., Wilson, D., White, V., et al. 2013, in Society of Photo-Optical Instrumentation Engineers (SPIE) Conference Series, Vol. 8864, 1
Baudoz, P., Rabbia, Y., & Gay, J. 2000, A&AS, 141, 319
Beuzit, J., Feldt, M., Dohlen, K., et al. 2008, in SPIE, Vol. 7014
Boccaletti, A., Schneider, J., Traub, W., et al. 2012, Experimental Astronomy, 1, 10.1007/s10686-012-9290-5
Brown, R. A. 2005, ApJ, 624, 1010
Brown, R. A., & Soummer, R. 2010, ApJ, 715, 122
Carlotti, A. 2013, A&A, 551, A10
Carlotti, A., N'Diaye, M., Riggs, A. J. E., et al. in prep.,
Carlotti, A., Pueyo, L., & Mawet, D. 2014, A&A, 566, A31
Carlotti, A., Vanderbei, R., & Kasdin, N. J. 2011, Optics Express, 19, 26796
Clampin, M., Melnick, G., Lyon, R., et al. 2006, in Society of Photo-Optical Instrumentation Engineers (SPIE) Conference Series, Vol. 6265, 1
Debes, J. H., Ygouf, M., Choquet, E., et al. submitted, to JATIS
Delacroix, C., Absil, O., Forsberg, P., et al. 2013, A&A, 553, A98
Dorrer, C., & Zuegel, J. D. 2007, Journal of the Optical Society of America B Optical Physics, 24, 1268
Feinberg, L. D., Jones, A., Mosier, G., et al. 2014, in Society of Photo-Optical Instrumentation Engineers (SPIE) Conference Series, Vol. 9143, 16
Floyd, R. W., & Steinberg, L. 1976, Proc. Soc. Inf. Disp, 75
Fourer, R., Gay, D. M., & Kernighan, B. W. 1990, Management Science, 36, 519
Galicher, R., Baudoz, P., Delorme, J. R., et al. 2014, in SPIE, Vol. 9143, 5
Gurobi Optimization, I. 2015, Gurobi Optimizer Reference Manual
Guyon, O., Hinz, P. M., Cady, E., Belikov, R., & Martinache, F. 2014, ApJ, 780, 171
Guyon, O., Martinache, F., Belikov, R., & Soummer, R. 2010a, ApJS, 190, 220
Guyon, O., Matsuo, T., & Angel, R. 2009, ApJ, 693, 75
Guyon, O., Pluzhnik, E. A., Kuchner, M. J., Collins, B., & Ridgway, S. T. 2006, ApJS, 167, 81
Guyon, O., & Roddier, F. J. 2000, in Proc. SPIE Vol. 4006, p. 377-387, Interferometry in Optical Astronomy, Pierre J. Lena; Andreas Quirrenbach; Eds., ed. P. J. Lena & A. Quirrenbach, Vol. 4006, 377–387
Guyon, O., Shaklan, S., Levine, M., et al. 2010b, in SPIE, Vol. 7731
Hicks, B. A., Lyon, R. G., Bolcar, M. R., Clampin, M., & Petrone, P. 2014, in Society of Photo-Optical Instrumentation Engineers (SPIE) Conference Series, Vol. 9143, 2
Hinkley, S., Oppenheimer, B. R., Zimmerman, N., et al. 2011, PASP, 123, 74
Kane, S. R., Ciardi, D. R., Gelino, D. M., & von Braun, K. 2012, MNRAS, 425, 757
Kasdin, N. J., Vanderbei, R. J., Spergel, D. N., & Littman, M. G. 2003, ApJ, 582, 1147
Kopparapu, R. K. 2013, ApJ, 767, L8
Kouveliotou, C., Agol, E., Batalha, N., et al. 2014, ArXiv e-prints, arXiv:1401.3741
Kuchner, M. J., & Traub, W. A. 2002, ApJ, 570, 900
Lyon, R. G., Hicks, B. A., Clampin, M., & Petrone, III, P. 2015, ArXiv e-prints, arXiv:1504.05747
Lyon, R. G., Clampin, M., Woodruff, R., et al. 2006, in IAU Colloq. 200: Direct Imaging of Exoplanets: Science & Techniques, ed. C. Aime & F. Vakili, 345–352

Macintosh, B., Graham, J. R., Ingraham, P., et al. 2014, Proceedings of the National Academy of Science, 111, 12661
Males, J. R., Belikov, R., & Bendek, E. 2015, ArXiv e-prints, arXiv:1510.02478
Marcy, G. W., Weiss, L. M., Petigura, E. A., et al. 2014, Proceedings of the National Academy of Science, 111, 12655
Martinez, P., Boccaletti, A., Kasper, M., Baudoz, P., & Cavarroc, C. 2007, A&A, 474, 671
Martinez, P., Dorrer, C., Aller Carpentier, E., et al. 2009, A&A, 495, 363
Martinez, P., Preis, O., Gouvret, C., et al. 2014, in SPIE, Vol. 9145, 4
Mas, M., Baudoz, P., Rousset, G., & Galicher, R. 2012, A&A, 539, A126
Mawet, D., Pueyo, L., Carlotti, A., et al. 2013, ApJS, 209, 7
Mawet, D., Riaud, P., Absil, O., & Surdej, J. 2005, ApJ, 633, 1191
Mawet, D., Pueyo, L., Lawson, P., et al. 2012, in Society of Photo-Optical Instrumentation Engineers (SPIE) Conference Series, Vol. 8442
Mawet, D., Milli, J., Wahhaj, Z., et al. 2014, ApJ, 792, 97
Mazoyer, J., Pueyo, L., Norman, C., et al. submitted, to JATIS
Mennesson, B. P., Shao, M., Levine, B. M., et al. 2003, in Society of Photo-Optical Instrumentation Engineers (SPIE) Conference Series, Vol. 4860, High-Contrast Imaging for Exo-Planet Detection., ed. A. B. Schultz, 32–44
Miller, K., Guyon, O., Codona, J., Knight, J., & Rodack, A. 2015, in Society of Photo-Optical Instrumentation Engineers (SPIE) Conference Series, Vol. 9605, 10
N'Diaye, M., Dohlen, K., Cuevas, S., et al. 2012, A&A, 538, A55
N'Diaye, M., Dohlen, K., Fusco, T., & Paul, B. 2013a, A&A, 555, A94
N'Diaye, M., Pueyo, L., & Soummer, R. 2015a, ApJ, 799, 225
N'Diaye, M., Choquet, E., Pueyo, L., et al. 2013b, in SPIE, Vol. 8864
N'Diaye, M., Choquet, E., Egron, S., et al. 2014, in SPIE, Vol. 9143, 27
N'Diaye, M., Mazoyer, J., Choquet, E., et al. 2015b, in Society of Photo-Optical Instrumentation Engineers (SPIE) Conference Series, Vol. 9605, 12
Newman, K., Guyon, O., Balasubramanian, K., et al. 2015, PASP, 127, 437
Otten, G. P. P. L., Snik, F., Kenworthy, M. A., Miskiewicz, M. N., & Escuti, M. J. 2014, Optics Express, 22, 30287
Petigura, E. A., Howard, A. W., & Marcy, G. W. 2013, Proceedings of the National Academy of Science, 110, 19273
Postman, M., Brown, T., Sembach, K., et al. 2012, Optical Engineering, 51, 011007
Pueyo, L., & Kasdin, N. J. 2007, ApJ, 666, 609
Pueyo, L., Kay, J., Kasdin, N. J., et al. 2009, Appl. Opt., 48, 6296
Pueyo, L., & Norman, C. 2013, ApJ, 769, 102
Redding, D. C., Feinberg, L., Postman, M., et al. 2014, in SPIE, Vol. 9143, 12
Roddier, F., & Roddier, C. 1997, PASP, 109, 815
Rouan, D., Riaud, P., Boccaletti, A., Clénet, Y., & Labeyrie, A. 2000, PASP, 112, 1479
Savransky, D., Kasdin, N. J., & Cady, E. 2010, PASP, 122, 401
Shaklan, S. B., & Green, J. J. 2006, Appl. Opt., 45, 5143
Silburt, A., Gaidos, E., & Wu, Y. 2015, ApJ, 799, 180
Singh, G., Martinache, F., Baudoz, P., et al. 2014, PASP, 126, 586
Sivaramakrishnan, A., & Lloyd, J. P. 2005, ApJ, 633, 528
Sivaramakrishnan, A., & Yaitskova, N. 2005, ApJ, 626, L65
Sivaramakrishnan, A., Soummer, R., Carr, G. L., et al. 2009, in Society of Photo-Optical Instrumentation Engineers (SPIE) Conference Series, Vol. 7440
Soummer, R. 2005, ApJ, 618, L161
Soummer, R., Aime, C., & Falloon, P. E. 2003a, A&A, 397, 1161
Soummer, R., Dohlen, K., & Aime, C. 2003b, A&A, 403, 369
Soummer, R., Pueyo, L., Ferrari, A., et al. 2009, ApJ, 695, 695
Soummer, R., Pueyo, L., Sivaramakrishnan, A., & Vanderbei, R. J. 2007, Optics Express, 15, 15935
Soummer, R., Sivaramakrishnan, A., Pueyo, L., Macintosh, B., & Oppenheimer, B. R. 2011, ApJ, 729, 144
Spergel, D., Gehrels, N., Baltay, C., et al. 2015, ArXiv e-prints, arXiv:1503.03757
Stapelfeldt, K. R., Brenner, M. P., Warfield, K. R., et al. 2014, in SPIE, Vol. 9143, 2
Stark, C. C., Roberge, A., Mandell, A., et al. 2015, ApJ, 808, 149
Stark, C. C., Roberge, A., Mandell, A., & Robinson, T. D. 2014, ApJ, 795, 122
Thomas, S. J., Belikov, R., & Bendek, E. 2015, ArXiv e-prints, arXiv:1501.01583
Trauger, J., Moody, D., & Gordon, B. 2013, in Society of Photo-Optical Instrumentation Engineers (SPIE) Conference Series, Vol. 8864, 12
Trauger, J., Stapelfeldt, K., Traub, W., et al. 2010, in SPIE, Vol. 7731
Vanderbei, R. 2012, Mathematical Programming Computation, 4, 53
Vanderbei, R. J. 2009, Linear Programming: Foundations and Extensions (Springer)
Vanderbei, R. J., Spergel, D. N., & Kasdin, N. J. 2003, ApJ, 599, 686
Ygouf, M., Pueyo, L., Soummer, R., et al. 2015, in Society of Photo-Optical Instrumentation Engineers (SPIE) Conference Series, Vol. 9605, 9
Zhao, F. 2014, in SPIE, Vol. 9143, 0
Zimmerman, N. T., Riggs, A. J. E., Kasdin, N. J., Carlotti, A., & Vanderbei, R. J. submitted, to JATIS